**PAPER • OPEN ACCESS**

# Domain wall motion at low current density in a synthetic antiferromagnet nanowire

To cite this article: Christopher E A Barker *et al* 2023 *J. Phys. D: Appl. Phys.* **56** 425002

View the article online for updates and enhancements.

# Domain wall motion at low current density in a synthetic antiferromagnet nanowire

**Christopher E A Barker**[1] (iD), **Simone Finizio**[2] (iD), **Eloi Haltz**[1,5] (iD), **Sina Mayr**[2,3],
**Philippa M Shepley**[1,4] (iD), **Thomas A Moore**[1] (iD), **Gavin Burnell**[1] (iD), **Jörg Raabe**[2] (iD)
and **Christopher H Marrows**[1,4,*] (iD)

[1] School of Physics and Astronomy, University of Leeds, Leeds LS2 9JT, United Kingdom
[2] Paul Scherrer Institut, 5232 Villigen PSI, Switzerland
[3] Laboratory for Mesoscopic Systems, Department of Materials, ETH Zurich, 8093 Zurich, Switzerland
[4] Bragg Centre for Materials Research, University of Leeds, Leeds LS2 9JT, United Kingdom

E-mail: c.h.marrows@leeds.ac.uk

CrossMark

## Abstract

The current-driven motion of magnetic domain walls (DWs) is the working principle of
magnetic racetrack memories. In this type of spintronic technology, high current densities are
used to propel DW motion in magnetic nanowires, causing significant wire heating that
corresponds to wasted energy. Synthetic antiferromagnets are known to show very fast DW
motion at high current densities, but lower current densities around onset of motion have
received less attention. Here we use scanning transmission x-ray microscopy to study the
response of DWs in a SAF multilayer to short current pulses. We observe that the DWs depin at
$(3.5 \pm 0.4) \times 10^{11} \, \mathrm{A \, m^{-2}}$ and move more quickly in response to 5 ns duration current pulses
than in comparable multilayers that lack antiferromagnetic coupling. The results suggest that
DWs in SAF structures are superior to conventional Néel DWs for low energy consumption
racetrack technologies.

Keywords: spin torque, domain wall, synthetic antiferromagnet

(Some figures may appear in colour only in the online journal)

## 1. Introduction

Magnetic domain walls (DWs) separate uniformly magnetized
domains in a ferromagnet. They are narrow regions where the
magnetization rotates between the directions in the domains
and both influence and respond to spin-polarised currents
[1]. The use of a spin-polarized electron flow and its res-
ulting torques on magnetic textures has been demonstrated
for driving DWs in magnetic wires [2]. New generations of
devices have been proposed based on these effects, such as the
so-called magnetic racetracks that can be used as storage-class
memories [3, 4] or for novel forms of information processing
[5–7]. In this type of technology, a stream of bits is encoded as
a series of domains separated by DWs in a magnetic nanowire,
which can be shifted along the wire using electrical current
pulses by means of the spin-torque mechanism. The DW vel-
ocity influences the speed of operation whilst the power dissip-
ated by the current pulse influences the energy consumption
of the device.

Initial versions of the magnetic racetrack were developed
using a simple strip of an in-plane magnetised soft magnetic

[5] Present address: Université Sorbonne Paris Nord, 99 Av. Jean Baptiste
Clément, 93430 Villetaneuse, France.
* Author to whom any correspondence should be addressed.

material such as Permalloy in which the DW motion was actuated by the volume spin-transfer-torque [3]. Further generations have incorporated developments such as multilayer wires with interface-induced effects such as perpendicular magnetic anisotropy (PMA) and Dzyaloshinskii–Moriya interactions (DMI) to enforce wall chirality [4], with DW motion now being driven by spin–orbit torques [8, 9].

Most recently, synthetic antiferromagnets (SAFs) [10] have been introduced as racetrack materials [11]. These systems are composed of two ferromagnetic (FM) layers coupled to each other antiferromagnetically through a non-magnetic spacer layer. The magnetic moments of the two layers compensate for each other leading to fast magnetization dynamics. In particular, very fast DW motion at several $100 \text{ m s}^{-1}$ for high current drives of a few TA m$^{-2}$ have been observed in these systems using a Ru spacer [12]. It has subsequently been shown that replacing the spacer material with Rh reduces the DW velocity [13], that DW velocity in a SAF can be controlled by means of iontronic gating [14], and that SAF nanowires can be connected to conventional FM wires and still transmit DWs [15]. A variety of effects related to curved tracks, disordered materials, and temperature fluctuations have been studied by means of micromagnetics [16].

Power consumption is a key constraint for such applications. In particular, fast motion at low current densities, just above the critical current density $J_c$ at which DWs depin from material or lithographic imperfections and can be set in motion, is critical. Here we study, using scanning transmission x-ray microscopy (STXM), the low current density dynamics of DWs around the onset of motion. We show that $J_c = (3.5 \pm 0.4) \times 10^{11} \text{ A m}^{-2}$ and that DWs move more quickly at lower current densities than in comparable conventional multilayers, i.e. ones that lack antiferromagnetic interlayer coupling and so are not SAFs. The multilayers that we study contain ten magnetic layers, showing that the advantages of the SAF structure extend beyond a pair of magnetic layers separated by a single spacer layer.

## 2. Methods and results

### 2.1. Multilayer growth and characterization

The SAF multilayers that we studied were deposited by magnetron sputtering in a chamber with a base pressure of $1.0 \times 10^{-9}$ mbar under a working pressure of $4.5 \times 10^{-3}$ mbar of Ar. Typical deposition rates, calibrated by x-ray reflectometry on test films, were $0.5 \text{ Å s}^{-1}$. Multilayers were grown simultaneously on x-ray transparent Si$_3$N$_4$ membranes for transmission microscopy and solid thermally oxidised Si substrates for magnetometry measurements.

The SAF multilayer stack that we studied is shown in figure 1(a). It features alternating layers of Co$_{68}$B$_{32}$ and Co$_{40}$Fe$_{40}$B$_{20}$, which form oppositely magnetised sublattices in the SAF ground state, owing to the indirect antiferromagnetic exchange through the Ru/Pt spacers, whose thicknesses were chosen to ensure this form of coupling [17]. There are five pairs of such layers in the completed stack. The FM layer thicknesses were selected so that they have equal and opposite
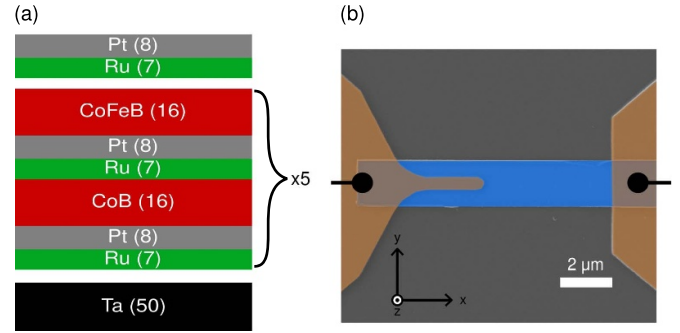


**Figure 1.** SAF multilayer nanowire. (a) SAF multilayer stack structure, with layer thicknesses given in Å; (b) SEM image of device.
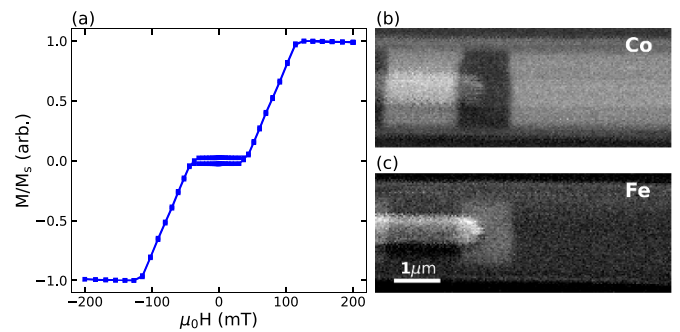


**Figure 2.** Magnetic characterization. (a) SQUID-VSM hysteresis loop with the field applied out-of-plane; (b),(c) STXM images showing opposite contrast at the Co and Fe $L_3$ edges, respectively.

magnetic moments. PMA and DMI are induced in the layers at their interfaces, predominantly by the heavy metal Pt.

Multilayers on the membranes were patterned into 2 $\mu$m wide wires by electron beam lithography and lift off, with current contacts at either end made from Cu, which is a light enough element to remain transparent to x-rays at the Co and Fe $L_3$ absorption edges. The design is similar to that used for skyrmion injection by Finizio *et al* [18], with a wide drain contact at the right hand end and a finger-shaped source contact on the left. We define conventional current flow in the positive direction as being out of the finger towards the right-hand end of the nanowire.

The multilayer on the solid substrate was characterized magnetically using superconducting quantum interference device vibrating sample magnetometry (SQUID-VSM). A magnetic hysteresis loop, acquired at room temperature and normalized to the saturation magnetization, is shown in figure 2. For applied fields smaller than about 45 mT the magnetization is constant and very small, less than 10% of the saturated value, showing that stack does indeed have a SAF ground state, and that the relative FM layer thicknesses are indeed close to the balance point.

We can estimate the strength of the AF coupling across the spacer from the saturation field $\mu_0 H_{sat} = 114 \pm 2$ mT as $J_{AF} = -\mu_0 H_{sat} M_s t_{FM}/4 = -17.8 \pm 0.3 \ \mu\text{J m}^{-2}$, for a saturation magnetisation-thickness product for the FM layers of

$M_s t_{FM} = 624 \pm 1\,\mu A$.[6] Note that in our balanced SAF this product takes the same value for both the CoFeB and CoB layers.

## 2.2. Magnetic imaging

The samples on membranes were imaged by means of STXM at the PolLux beamline at the Swiss Light Source [19]. Images of the region of the nanowire close to the source contact are shown figures 2(b) and (c), acquired using x-ray photons with energies at the Co and Fe $L_3$ absorption edges, respectively. Since magnetic contrast in this technique arises owing to the x-ray magnetic circular dichroism effect (XMCD), we can separately probe the magnetism of these two elements by this means. The x-ray beam passed through the multilayer at normal incidence, and so the magnetic contrast is proportional to the out-of-plane component of the magnetization, $M_z$, with dark contrast signifying magnetization that points into the plane of the paper and bright contrast out of the plane of the paper.

In each image a domain that spans the width of the wire can be observed under the tip of the source contact, appearing as a band of dark contrast in figure 2(b) and a band of light contrast in figure 2(c). In this case we are imaging the as-patterned state, prior to the application of any fields or current pulses, although similar domain structures could be created by applying current pulses to a uniformly magnetised nanowire. Since only one sublattice of FM layers, made from CoFeB, contains Fe, only those layers contribute to the contrast in figure 2(c). Meanwhile, the Co content of the CoB layers is higher than that of the CoFeB layers, so that although the contrast in figure 2(b) arises from both sublattices, it will be predominantly from the CoB sublattice. The fact that the contrast is of opposite sign in this pair of images confirm the SAF state, with CoB and CoFeB sublattices being oppositely magnetized. All pairs of images taken at the Co and Fe edges that we took in the course of these experiments always show equivalent oppositely magnetised states, indicating that the interlayer exchange coupling is strong enough to enforce opposite domain structures in the two sublattices.

We have studied the response of such DWs to nominally 5 ns duration pulses of electrical current injected into the magnetic wire. The pulses were generated with a Keysight M8195A arbitrary waveform generator (64 GSa s$^{-1}$ sampling rate) combined with a SHF-826 H amplifier. An oscilloscope (50 $\Omega$ terminated) trace of such a pulse after it has passed through the wire is shown in figure 3(a). The pulse retains a high degree of squareness with modest ringing after the pulse, which peaks at a current density $J \sim 3.0 \times 10^{11}$ A m$^{-2}$. The current density was calculated using the rectangular cross-sectional area of the entire nanowire, which is the area of the DW through which the current passes. On this basis we estimate the error bar $\delta J/J \approx 0.09$. The current distribution in
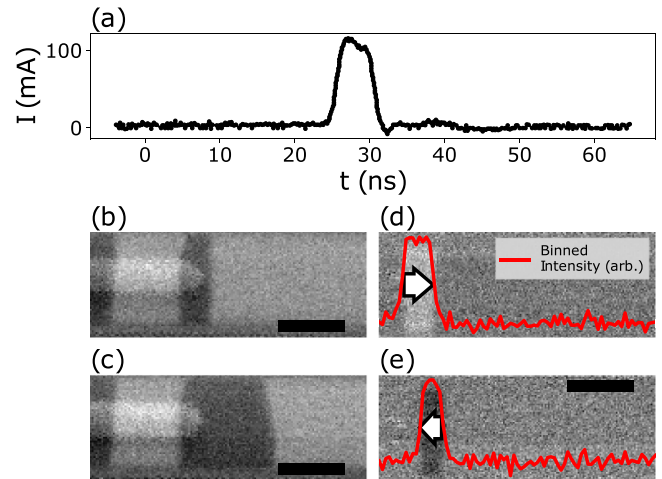


**Figure 3.** DW motion under current pulses. (a) pulse from oscilloscope. (b), (c) STXM images showing before and after images of DW motion, (d), (e) difference images showing DW motion and fitting.

a similar structure with the same geometry was previously calculated using finite element modelling [18]. The current density becomes substantially uniform after a rather short distance from the tip of the Cu finger electrode, less than 500 nm.

Figures 3(b) and (c) show STXM images acquired before and after the application of five such pulses, separated by a few seconds to allow for a complete cooling of the magnetic wire. The positions of the DWs are marked with dashed red lines. The left-hand DW is unaffected by the current pulses, as expected since the current is shunted by the overlying Cu finger electrode. On the other hand, the right hand wall moves away from the finger electrode, in the direction of the conventional current flow, indicating spin–orbit torques as the most likely mechanism to drive the motion: this is the usual direction of motion for DWs in a FM layer on a Pt layer, owing to the combination of DMI-induced left-handed DW chirality and spin Hall effect arising from that material [20]. The movement is a distance of a few hundred nm, and is not completely uniform across the wire, with the DW moving further along the edge of the wire in the lower part of the image than the edge in the upper part in this case.

This sort of DW tilting under spin–orbit torques has been previously observed in Co/Ni/Co multilayers with DMI [21], subsequently shown to be an intrinsic effect of the dynamics of DWs under DMI [22]. The model of Boulle *et al* [22] predicts that the tilt angle should be $\propto M_s$ and so ought to be zero for a SAF. Whilst it is quite common for us to see some tilt in our images like the example in figure 3(c), the tilt angle is quite variable and can be of either sign. Based on these considerations, we think it is likely that the tilts we observe are extrinsic and arise stochastically from pinning of the DWs at defects, particularly on lithographic imperfections at the edges of our nanowires.

In order to study this DW motion in a more systematic way, we acquired a series of images using positive helicity photons at the Co $L_3$ edge before and after series of current pulses

---

[6] Note that here we follow the convention of using the symbol $J_{AF}$ to denote this interlayer exchange constant, not to be confused with the current density driving the DW motion $J$. We also adopt the sign convention that $J_{AF} < 0$ for antiferromagnetic coupling.

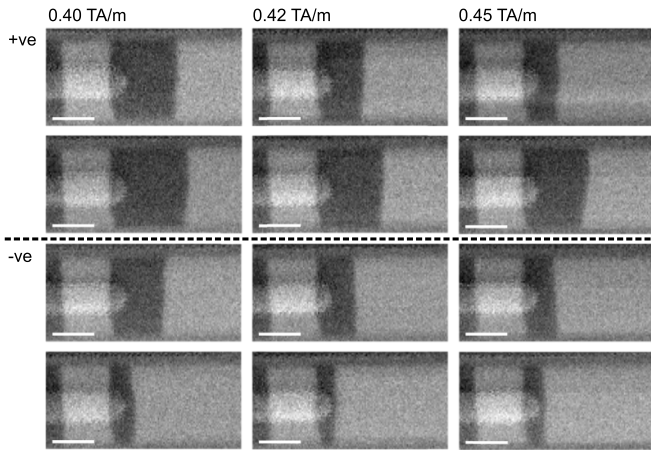J. Phys. D: Appl. Phys. **56** (2023) 425002

C E A Barker *et al*



**Figure 4.** Selected images DW motion for various values of current density *J* applied in the positive and negative sense for 5 ns. We show pairs of images acquired at the Co $L_3$ edge before and after the pulse. In each case the scale bar is 1 $\mu$m.
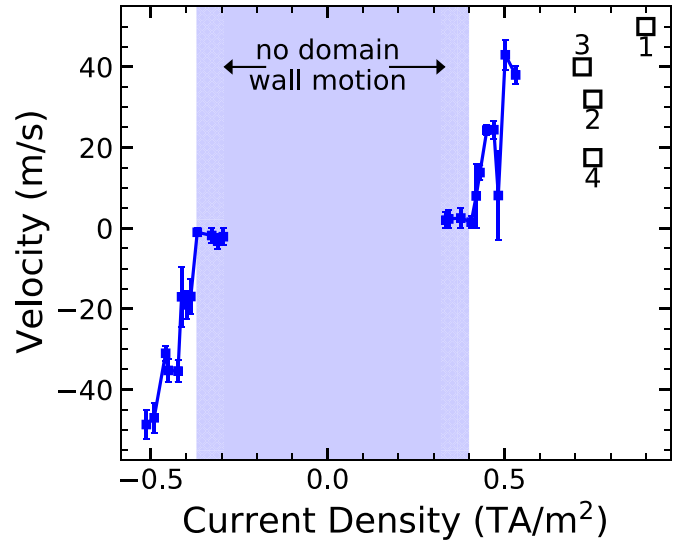


**Figure 5.** DW velocity vs current density. The solid blue region in the centre of the plot shows the range of current density for which no DW motion was ever observed. On each side is a hatched blue region, in this range of current densities we observed occasional DW motion. Black data points are derived from prior work on comparable CoB-based samples: data point 1 is derived from data reported in [23], data points 2 and 4 from [24], and data point 3 from [25].

of different *J* but with the same duration, 5 ns. Examples of images of DW motion for different current densities in the positive and negative direction are shown in figures 4. These DWs all appear similar and representative of all the DWs that we observed. Subtracting pairs of these images yields difference images: examples are shown in figure 3(d) and (e). These difference images show the area swept out by the DW during motion driven by sequences of 10 positive polarity (d), and then 10 negative polarity (e) pulses of $6.35 \times 10^{11}$ A m$^{-2}$. Bright contrast in the difference corresponds to rightward motion, and dark contrast to leftward motion.

### 2.3. DW velocity

To determine the distance traveled by the DW under the influence of these pulses, the contrast values in a column of pixels across the wire were binned together. The red lines in figures 3(c) and (d) show how this binned contrast varies along the length of the wire, with clear excursions away from the background level in the region where the DW motion has occurred. The distance traveled by the DW is then taken to be the full-width at half maximum value of this excursion, giving the average value for distance traveled in the case of non-uniform wall motion.

We determined the velocity as this distance divided by the total nominal duration of the pulses in the pulse sequence, and so use this term to refer to the average velocity of the DW during its motion. Here we have only included data where the DW position is at least 500 nm from the tip of the electrode where the current distribution across the wire width can be expected to be uniform.

The velocities derived from this analysis are plotted as a function of current density in figure 5. There is a coloured region of low *J* where there is no observable DW motion. In this region we show no data points. Once |*J*| exceeds a value of $(3.0 \pm 0.1) \times 10^{11}$ A m$^{-2}$ then DW motion in the direction of conventional current flow begins to take place. At first,

DW motion is not observed for every pulse, and we show a hatched region where there is stochastic DW motion, which extends a further $0.8 \times 10^{11}$ A m$^{-2}$. We define the critical current density for the onset of motion as the middle of this region stochastic region, and so $J_c = (3.5 \pm 0.4) \times 10^{11}$ A m$^{-2}$.

Beyond this region, in the part of the graph with a white background, we observed DW motion every time we applied a pulse. There, the DW velocity rises as the current becomes stronger, and reaches a value exceeding 40 m s$^{-1}$ at the maximum measured current density of a little over $J = 5 \times 10^{11}$ A m$^{-2}$.

High current densities can induce transient heating of the nanowire. Nevertheless, measuring the transient temperature rise of a nanoscale structure during a current pulse that is only a few ns long is a challenging experiment. We have tackled this challenge by performing time-resolved measurements of the change in XMCD contrast during the current pulse.

The time-resolved measurements were performed by first saturating the sample in a FM state by applying an out-of-plane magnetic field of 200 mT. In order to allow sufficient time for the sample to cool down to room temperature (therefore simulating the quasi-static experiments), while retaining a reasonable measurement time, we performed the time-resolved measurements with a pulse waveform period of 200 ns, injecting first a positive pulse and then a negative pulse within that period leading to temperature excursions 100 ns apart. For both pulses, a current density of $3.7 \times 10^{11}$ A m$^{-2}$ was injected, and the pulses were 5 ns wide, reproducing the conditions of the quasi-static experiments close to the DW depinning threshold. The time-resolved measurements were performed with a temporal resolution of 200 ps at the Fe $L_3$
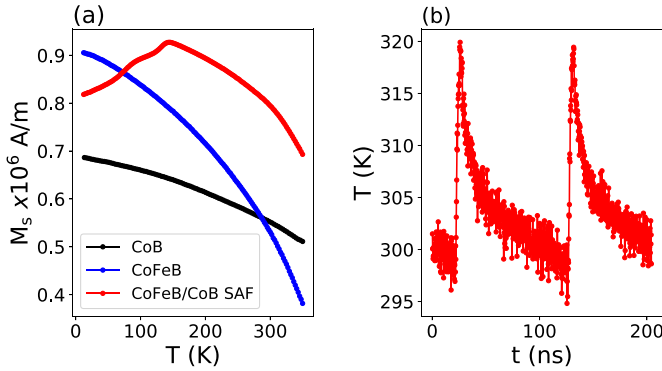
**Figure 6.** Transient heating of the nanowire. (a) Temperature dependence of the saturation magnetization for single layers of CoFeB and CoB, nominally identical to those in the SAF, as well as a full SAF structure, under an applied perpendicular field of 200 mT. This field was not strong enough to overcome the antiferromagnetic coupling and maintain a saturated state for the SAF at low temperatures, resulting in an apparent drop in $M_s$. (b) Time-resolved XMCD measurements at the Fe $L_3$ edge, converted to the temperature of the wire using the SQUID-VSM data for CoFeB in panel (a).

edge, i.e. probing the CoFeB layer. As the CoFeB layer is uniformly magnetized, the only influence caused by the current pulse is to be attributed to the reduction of the XMCD contrast caused by the heating induced by the pulse. At the pulse conditions described above, a drop of about 10% of the XMCD contrast at room temperature was observed. By comparing the measurements with $M_s(T)$ curves measured by SQUID-VSM on witness samples that contained identical magnetic layers to those in the SAF, shown in figure 6(a), we could determine that the measured drop in XMCD contrast corresponds to a heating of the sample of about 20 K, as shown in figure 6(b). This is a modest temperature rise that is unlikely to significantly affect the depinning current density $J_c$.

## 3. Discussion

To compare the results we have obtained here on DWs in SAF multilayers with conventional ones, we have performed a meta-analysis on prior work on STXM imaging of current-driven DW motion in conventional multilayers based around a Pt/CoB/Ir repeat unit that have a FM-aligned ground state [23–25]. Data points obtained from those previous works are also plotted in figure 5. We can see that comparable velocities were reached in those experiments, but substantially higher current densities were required to do so. Our results mirror a reduction in $J_c$ seen previously in in-plane magnetized SAFs when compared to simple Permalloy wires [26].

The depinning current $J_c$ observed here is also about half of that reported by Yang *et al* in reference [12] for a two-layer SAF. In that case, only one of the two layers had an interface with a heavy metal–Pt–to supply both DMI to stabilise the Néel DW structure and spin–orbit torque to drive the motion of those walls. As shown by the work of Alejos *et al* [16], this leads to a low coupling regime where the walls cannot be driven together as a composite object. Thus, we expect the DW

velocity to be independent of the strength of the coupling so long as it is strong enough to maintain the array of DWs in all the separate layers to act as a single rigid DW under differential drives for different layers. Since every layer in our stack has the same Pt underlayer, we expect that the spin Hall current that drives the DW motion will be similar in all of our layers, and all will have the Néel structure enforced to a similar extent. This means that differential drives will be small and so in this case this regime will extend down to quite weak AF coupling: important since our value of $J_{AF}$ is considerably smaller then that in in reference [12] owing to those additional Pt layers in the spacers. When comparing images taken on the Co and Fe edges we saw no evidence for uncoupled walls. It is worth noting that we made our FM layers differ only for the experimental convenience of being able to distinguish them by means of the element specificity of the soft x-ray technique. If needed in an application, every layer can be made identically in our approach.

We should also like to briefly discuss DW motion in rare earth-transition metal ferrimagnets, materials in which the 4$f$ and 3$d$ moments align antiferromagnetically and so are another means of forming a zero moment structure. Field driven motion faster than 1 km s$^{-1}$ for fields $\sim$100 mT has been observed in GdFeCo [27]. Similarly fast current-driven motion has been reported in a Pt/GdCo/TaO$_x$ trilayer for a current drive $J \sim 2 \times 10^{12}$ A m$^{-2}$ [28], and up to 80 m s$^{-1}$ at $J \sim 0.45 \times 10^{12}$ A m$^{-2}$ in Pt/CoTb/SiN$_x$ [29]. All of these results rely on being sufficiently close to the temperature at which the angular momentum of the two sublattices is compensated, $T_A$, which limits the operating temperature range when this approach is taken. Moreover, since the $g$-factors of the rare earth and transition metal elements differ, the temperature at which the magnetic moments are compensated, $T_M$, can differ, meaning that there can be a finite net moment at the operating point which will make the system susceptible to interference from stray magnetic fields.

## 4. Conclusion

To summarise, we have studied DW motion in a SAF multilayer using STXM. We find motion at comparable velocities to conventional perpendicularly magnetised multilayers, but at reduced current densities that imply power dissipation reduced by up to 50%. We also find a critical current density $J_c$ that is substantially less than that in a two-layer SAF, indicating the advantages of a stack design where every magnetic layer is subject to a spin–orbit torque. Our results offer promise for low power consumption DW racetrack technologies as well as suggesting that the motion of skyrmions in such SAFs [30–32] is also likely to only require modest current densities.

## Data availability statement

The data that support the findings of this study are openly available at the following URL/DOI: https://doi.org/10.5518/1380 [33].

## Conflict of interest

The authors declare no conflict of interest.

## ORCID iDs

Christopher E A Barker ● https://orcid.org/0000-0001-7266-3223
Simone Finizio ● https://orcid.org/0000-0002-1792-0626
Eloi Haltz ● https://orcid.org/0000-0001-7133-9800
Philippa M Shepley ● https://orcid.org/0000-0003-1240-593X
Thomas A Moore ● https://orcid.org/0000-0001-6443-2556
Gavin Burnell ● https://orcid.org/0000-0002-9486-0639
Jörg Raabe ● https://orcid.org/0000-0002-2071-6896
Christopher H Marrows ● https://orcid.org/0000-0003-4812-6393

## References

[1] Marrows C H 2005 *Adv. Phys.* **54** 585–713
[2] Yamaguchi A, Ono T, Nasu S, Miyake K, Mibu K and Shinjo T 2004 *Phys. Rev. Lett.* **92** 077205
[3] Parkin S S P, Hayashi M and Thomas L 2008 *Science* **320** 190–4
[4] Parkin S S P and Yang S H 2015 *Nat. Nanotechnol.* **10** 195–8
[5] Luo Z, Hrabec A, Dao T P, Sala G, Finizio S, Feng J, Mayr S, Raabe J, Gambardella P and Heyderman L J 2020 *Nature* **579** 214–8
[6] Vakili H, Sakib M N, Ganguly S, Stan M, Daniels M W, Madhavan A, Stiles M D and Ghosh A W 2020 *IEEE J. Explor. Solid-State Computat. Devices Circuits* **6** 107–15
[7] Ollivier S, Longofono S, Dutta P, Hu J, Bhanja S and Jones A K 2022 CORUSCANT: fast efficient processing-in-racetrack memories *2022 55th IEEE/ACM Int. Symp. on Microarchitecture (MICRO)* pp 784–98
[8] Emori S, Bauer U, Ahn S M, Martinez E and Beach G S D 2013 *Nat. Mater.* **12** 611–6
[9] Ryu K S, Thomas L, Yang S H and Parkin S 2013 *Nat. Nanotechnol.* **8** 527–33
[10] Duine R A, Lee K J, Parkin S S P and Stiles M D 2018 *Nat. Phys.* **14** 217–9
[11] Yang S H and Parkin S 2017 *J. Phys.: Condens. Matter* **29** 303001
[12] Yang S H, Ryu K S and Parkin S S P 2015 *Nature Nanotechnol.* **10** 221–6
[13] Cohen A, Jonville A, Liu Z, Garg C, Filippou P C and Yang S H 2020 *J. Appl. Phys.* **128** 053902
[14] Guan Y, Zhou X, Li F, Ma T, Yang S H and Parkin S S P 2021 *Nat. Commun.* **12** 5002
[15] Yoon J, Yang S H, Jeon J C, Migliorini A, Kostanovskiy I, Ma T and Parkin S S P 2022 *Nat. Nanotechnol.* **17** 1183–91
[16] Alejos O, Raposo V, Sanchez-Tejerina L, Tomasello R, Finocchio G and Martinez E 2018 *J. Appl. Phys.* **123** 013901
[17] Lavrijsen R, Fernández-Pacheco A, Petit D, Mansell R, Lee J H and Cowburn R P 2012 *Appl. Phys. Lett.* **100** 052411
[18] Finizio S, Zeissler K, Wintz S, Mayr S, Weßels T, Huxtable A J, Burnell G, Marrows C H and Raabe J 2019 *Nano Lett.* **19** 7246–55
[19] Raabe J *et al* 2008 *Rev. Sci. Instrum.* **79** 113704
[20] Kuepferling M, Casiraghi A, Soares G, Durin G, Garcia-Sanchez F, Chen L, Back C H, Marrows C H, Tacchi S and Carlotti G 2022 Measuring interfacial Dzyaloshinskii-Moriya interaction in ultra-thin magnetic films (arXiv:2009.11830v3)
[21] Ryu K S, Thomas L, Yang S H and Parkin S S P 2012 *Appl. Phys. Express* **5** 093006
[22] Boulle O, Rohart S, Buda-Prejbeanu L D, Jué E, Miron I M, Pizzini S, Vogel J, Gaudin G and Thiaville A 2013 *Phys. Rev. Lett.* **111** 217203
[23] Finizio S, Wintz S, Zeissler K, Sadovnikov A V, Mayr S, Nikitov S A, Marrows C H and Raabe J 2018 *Nano Lett.* **19** 375–80
[24] Finizio S, Wintz S, Mayr S, Huxtable A J, Langer M, Bailey J, Burnell G, Marrows C H and Raabe J 2020 *Appl. Phys. Lett.* **117** 212404
[25] Finizio S, Wintz S, Mayr S, Huxtable A J, Langer M, Bailey J, Burnell G, Marrows C H and Raabe J 2020 *Appl. Phys. Lett.* **116** 182404
[26] Lepadatu S *et al* 2017 *Sci. Rep.* **7** 1640
[27] Kim K J *et al* 2017 *Nat. Mater.* **16** 1187–92
[28] Caretta L *et al* 2018 *Nat. Nanotechnol.* **13** 1154
[29] Siddiqui S A, Han J, Finley J T, Ross C A and Liu L 2018 *Phys. Rev. Lett.* **121** 057701
[30] Dohi T, DuttaGupta S, Fukami S and Ohno H 2019 *Nat. Commun.* **10** 5153
[31] Legrand W, Maccariello D, Ajejas F, Collin S, Vecchiola A, Bouzehouane K, Reyren N, Cros V and Fert A 2020 *Nat. Mater.* **19** 34
[32] Chen R *et al* 2020 *Nano Lett.* **20** 3299
[33] Barker C E A, Finizio S, Haltz E, Mayr S, Shepley P M, Moore T A, Burnell G, Raabe J and Marrows C H 2023 Domain wall motion at low current density in a synthetic antiferromagnet nanowire (University of Leeds) (https://doi.org/10.5518/1380)